A COTS-Based Microwave Imaging System for Breast-Cancer Detection

Original
A COTS-Based Microwave Imaging System for Breast-Cancer Detection / Casu, M.R., Vacca, M., TOBON VASQUEZ, J.A., Pulimeno, A., Sarwar, I., Solimene, R., Vipiana, F.. - In: IEEE TRANSACTIONS ON BIOMEDICAL CIRCUITS AND SYSTEMS. - ISSN 1932-4545. - STAMPA. - 11:4(2017), pp. 804-814. [10.1109/TBCAS.2017.2703588]

Publisher:
IEEE

Published
DOI:10.1109/TBCAS.2017.2703588

A COTS-Based Microwave Imaging System for Breast-Cancer Detection

Mario R. Casu, *Member, IEEE,* Marco Vacca, Jorge A. Tobon, Azzurra Pulimeno, Imran Sarwar,
Raffaele Solimene, and Francesca Vipiana, *Senior Member, IEEE*

***Abstract*—Microwave Imaging is an emerging breast cancer diagnostic technique, which aims at complementing already established methods like mammography, magnetic resonance imaging, and ultrasound. It offers two striking advantages: no-risk for the patient and potential low-cost for national health systems. So far, however, the prototypes developed for validation in labs and clinics used costly lab instruments, such as a Vector Network Analyzer (VNA). Moreover, the CPU time required by complex image reconstruction algorithms may not be compatible with the duration of a medical examination. In this paper, both these issues are tackled. Indeed, we present a prototype system based on low-cost and off-the-shelf microwave components, custom-made antennas, and a small form-factor processing system with an embedded Field-Programmable Gate Array (FPGA) for accelerating the execution of the imaging algorithm. We show that our low-cost system can compete with an expensive VNA in terms of accuracy, and it is more than 20x faster than a high-performance server at image reconstruction.**

***Index Terms*—Breast cancer detection, microwave imaging, components off-the-shelf.**

I. INTRODUCTION

MICROWAVE Imaging (MI) for breast cancer detection [1] is being considered as a diagnostic tool that can complement well-established methods like mammography [2] and magnetic resonance imaging (MRI) [3][4][5]. This is because MI offers a different perspective of the breast, being sensitive to the dielectric contrast between the normal and diseased tissues rather than the density [6]. Tumor tissues are characterized by a higher dielectric constant than healthy tissues [7]. Also, MI presents some advantages over mammography: being free from ionizing radiations, MI is risk-free for the patient and therefore can be repeated much more frequently; the patient is more comfortable because MI does not require any painful compression of the breast during the examination; MI is recommended also for younger women with dense breasts [8][9]. The main advantage of MI over the very expensive MRI, which is sometimes proposed as a follow-up procedure in tumor treatments, is instead its low cost. For these reasons, MI is an ideal candidate for large scale screening campaigns and post-treatment cancer surveillance [10].

Two main approaches for MI have been proposed so far, *Ultra Wide-Band (UWB) Radar* and *Tomography*.

The radar approach [11] belongs to the class of linear scattering techniques and consists in acquiring and processing UWB pulses scattered back by the patient's breast tissues in order to create a map of the reflected energy [12]. Due to the dielectric contrast, a tumor will cause a highly energetic spot in the image. Therefore, this is basically a *detection* method. To use the UWB radar approach in the time-domain, ad-hoc new integrated circuits (ICs) need to be developed [13][14][15][16]. It is possible to use this approach in the frequency-domain and reconstruct the UWB pulses via FFT [17], an approach usually referred in the literature as Stepped-Frequency Continuous Wave (SFCW) [18]. In this second case, besides developing new ICs [18][19], one can use sophisticated laboratory microwave tools [20], which have the necessary flexibility to handle a large bandwidth with the required precision and accuracy. In any case, none of these implementations of the UWB radar approach can be classified as low-cost.

The tomographic approaches [21][22] aim to reconstruct the dielectric breast profile by collecting the scattered field at a single or few selected frequencies [6][23]. The main limitation of this approach, however, is in the processing part as a non-linear and ill-posed inverse problem has to be solved [24]. Apart from convergence and stability, the main issue is the execution time, because non-linear inversions may take days of CPU.

Our approach to MI is different than both a radar and a tomographic approach. We adopted as imaging algorithm Interferometric- MUltiple SIgnal Classification (I-MUSIC) [25], which belongs, like radar methods, to the linear scattering class of imaging techniques. Differently from radar techniques, however, I-MUSIC does not require a large bandwidth to detect the most scattering points inside the breast. In fact, we developed a system that works in the frequency domain and uses only eleven discreet frequencies chosen in a 200-MHz bandwidth between 1.4 and 1.6 GHz. Since low-cost components off-the-shelf (COTS) are available in this frequency range, there is no need for new ICs. In addition, since it is not a tomographic approach, I-MUSIC allows us to avoid the processing issues of non-linear inversions[1]. A chief feature of I-MUSIC is that the imaging algorithm does not

---

Manuscript received Month XX, 20XX; revised Month YY, 20YY.

This work was supported by the Italian Ministry of University and Research under FIRB project MICENEA and by COST Action TD1301 MiMed.

M.R. Casu, I. Sarwar, J.A. Tobon, M. Vacca, and F. Vipiana are with the Department of Electronics and Telecommunications, Politecnico di Torino, I-10129 Torino, Italy e-mail: {mario.casu,francesca.vipiana}@polito.it.

A. Pulimeno was with the Department of Electronics and Telecommunications, Politecnico di Torino. She is now with Imagination Technologies, Hertfordshire WD4 8LZ, U.K.

R. Solimene is with the Department of Information Engineering, Second University of Naples, 81031 Aversa, Italy.

[1] Note, however, that the RF COTS of our system could be used also for tomographic approaches, which we did not experiment with.

require a pre-characterized response of the antennas, which has two important consequences. The first advantage is a reduction of costs and time for testing and calibration. The second advantage is that in practical cases the response of the antennas is unknown, since they are deployed in close-proximity of an unknown scatterer. This last issue, which complicates further the reconstruction problem in standard linear inversion methods, is avoided altogether in I-MUSIC.

The I-MUSIC algorithm, albeit faster than a non-linear inversion, may still require a CPU time unacceptable for a standard clinical scenario, especially if run on an embedded processor. To speed-up the execution of the most computationally intensive kernel of I-MUSIC, we pair the embedded processor with a hardware accelerator running in a field-programmable gate array (FPGA).

To evaluate the performance of our system prototype we carried out experiments on different kinds of 2D and 3D breast and tumor phantoms placed in a tank with different coupling liquids. We also designed and fabricated low-cost printed antennas that are matched when immersed in these liquids. We obtain results comparable in terms of accuracy to what a sophisticated microwave equipment can achieve, but at a small fraction of the cost. Moreover, our FPGA-enhanced embedded platform accelerates the image reconstruction algorithm by more than 20x compared to a powerful multicore CPU.

In summary, these are our main original contributions:

- We show that it is possible to build a low-cost MI system for breast-cancer detection with accuracy comparable to RF instruments using COTS and printed antennas.
- We show that I-MUSIC can run on an embedded platform, enhanced with an FPGA, more than 20x faster than on a server-grade CPU.

All the reported results have been obtained using an existing MI algorithm, I-MUSIC, whose detection effectiveness has been proven already [25][26].

This is the paper organization. After a brief description of the algorithm and the related work in Sec. II, we describe our prototype and the tumor phantoms in Sec. III, and report the experimental results in Sec. IV. Our conclusions are in Sec. V.

II. BACKGROUND AND RELATED WORK

We briefly describe I-MUSIC, the algorithm that we use in our system. The details can be found in [25]. I-MUSIC consists of two steps: clutter removal and breast image generation.

The clutter is mainly due to a large scattering at the coupling-medium/skin interface. To remove it, I-MUSIC uses a subspace-projection method based on the singular value decomposition (SVD) of the data matrix. Assume that the scattered field is sensed at N different frequencies by A different antenna pairs operating in bistatic mode (one transmitting and one receiving). The matrix of the acquired complex data (i.e. real and imaginary part of the field) is organized in N rows and A columns. This matrix is transformed via SVD and the projections relative to the two dominant singular values are discarded to remove the clutter.

The so-obtained decluttered matrix S_d is the input to the image generation algorithm. For each frequency f, the eigenvectors and eigenvalues $[V, D]$ of the correlation matrix $\mathbf{R} = S_d^f \cdot (S_d^f)^H$ are computed, where S_d^f is the fth row of the $N \times A$ decluttered matrix S_d. For each pixel of the output image, identified by the row and column indexes (u, v), through a Hermitian inner product the dominant eigenvector $V_{\max}$ of $\mathbf{R}$ is multiplied with an array of Green functions, W. These functions model the propagation between the A antenna pairs and the point in the scanned region that corresponds to the pixel in question. The Euclidian norm of this Hermitian product is the function $F(u, v, f)$, which is computed for all N frequencies (i.e. on all rows of S_d).

All frequency components of $F(u, v, f)$ are combined together as $\prod_f (1 - F(u, v, f)^2)$ and the inverse of this product $P(u, v)$ is the matrix containing the output image. Note that the product of single-frequency contributions produces a sort of constructive interference, which strongly emphasizes the actual tumor response and tends to reduce spurious artifacts.

I-MUSIC has been numerically and experimentally assessed in [26] using a Vector Network Analyzer (VNA) for probing a breast phantom and collecting the corresponding scattered field. Also, a PC has been used for processing the acquired data. In this paper, instead, we present the first attempt to build an ad-hoc and low-cost system, for which we showed preliminary promising results in [27][28][29].

There have been previous attempts to avoid VNAs, especially for UWB radar systems working directly in the time domain [30]. While the authors of [30] try to avoid custom components, others propose the implementation of ad-hoc CMOS ICs working in time domain, with the aim of improving the performance over commercial components [14][31][15][16]. One of the issues with these UWB time-domain methods is the need for complex calibration schemes to remove the clutter. This problem has been recently addressed and a new signal processing method has been proposed [32].

Working in the frequency domain, as VNAs do, has a distinctive advantage over working in the time domain: for each frequency, the signal-to-noise ratio is as high as that of a narrow-band system. In order to work in frequency domain while avoiding the use of VNAs, researchers propose dedicated CMOS ICs [18]. If the goal is to reduce cost, however, we believe that COTS working in frequency domain can be used, as we show in this paper.

III. SYSTEM ARCHITECTURE AND DESIGN

Fig. 1 is a schematic representation of our prototype system, which is also helpful to explain the principle upon which the entire MI system is based.

A *transmitter* generates a radiofrequency (RF) signal, whose frequency is programmed by the ARM embedded processor in the *Zynq System-on-Chip (SoC)*. A cable connects the transmitter with an antenna that irradiates a tank with the signal *RF out* amplified by a variable-gain amplifier (VGA). The tank contains a coupling liquid and a breast phantom, which mimics the various breast tissues (adipose, fibro-glandular, and tumor) with liquids of different dielectric properties. The scattered signal is received by another antenna, which conveys the signal *RF in* to a *direct conversion (DC) receiver*. The in-phase (I)

This is the author's version of an article that has been published in this journal. Changes were made to this version by the publisher prior to publication.
The final version of record is available at http://dx.doi.org/10.1109/TBCAS.2017.2703588

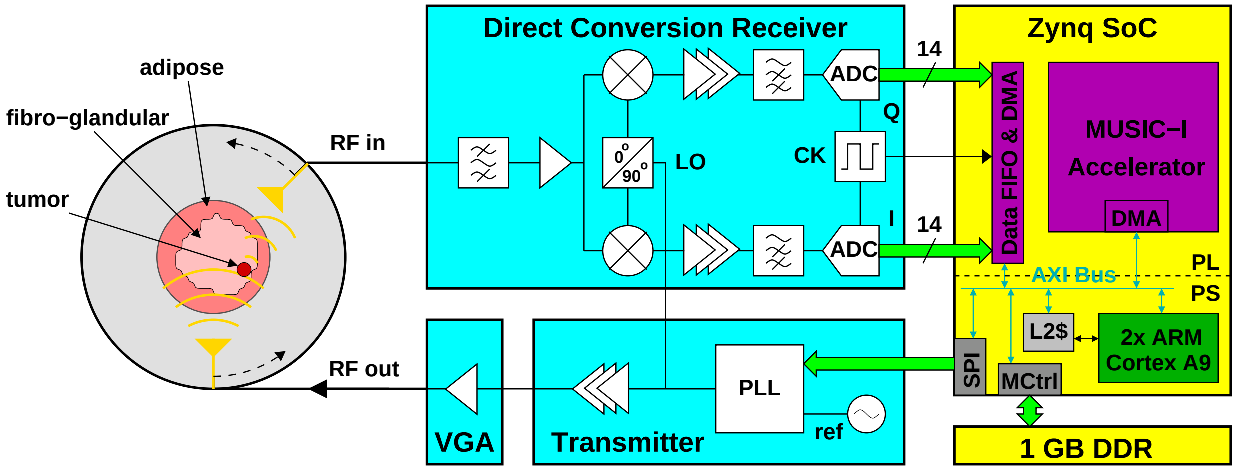

Fig. 1. Architecture of our prototype system for breast-cancer detection using Microwave Imaging.

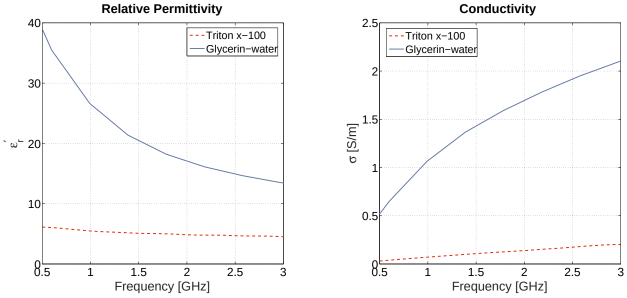

(a) **(b)**

Fig. 2. (a) Relative permittivity and (b) conductivity of the coupling liquids: 80-20% glycerin-water mixture (solid lines) and Triton x-100 (dashed lines).

and quadrature (Q) outputs of the DC receiver are digitized and sent to the SoC.

A brushless motor rotates around a circle the two antennas, which keep a fixed angle between them (135° in Fig. 1). A set of pre-determined positions is chosen, and for each position a set of measurements at different frequencies are taken. Finally, the received signals are elaborated inside the Zynq SoC via the I-MUSIC algorithm, which produces an image highlighting the position of the scatterers in the scene.

Notice that the RF parts colored in light-blue in Fig. 1 could be replaced by a conventional and expensive VNA. Likewise, the elaboration parts colored in yellow in Fig. 1 could be replaced by a conventional PC. Our aim, though, is to prove that an implementation using components off-the shelf (COTS) is not only feasible and cheaper, but that it can achieve a comparable detection performance.

In the following we discuss in detail the various parts of the system in Fig. 1.

A. Measurement Tank with Coupling Liquids and Antennas

We experimented with two different coupling liquids proposed in the literature that have different properties.

The first coupling liquid is obtained by mixing glycerin (80%) and water (20%) and was proposed for the first time in [33]. We report in Fig. 2 (solid lines) the dielectric properties of the glycerin-water mixture measured in the frequency range 0.5-3 GHz; our measurements are in good agreement with the dielectric properties reported in [33, Fig. 6]. We verified that this coupling liquid is not only easy to reproduce, but most of all stable over time, which simplifies the measurements procedure and improves the repeatability of the experiments. Compared to other coupling liquids proposed in literature, this mixture presents a higher conductivity (Fig. 2.(b)), which implies a higher signal attenuation. This attenuation can be useful to eliminate the effect of multipaths and to provide an appropriate impedance matching to minimize signal attenuation from reflections at the breast/liquid surface [33]; however, it also requires a measurement system with a high dynamic range and low-noise, especially when the transmitted signal level is low.

The second coupling liquid used in our experiments is Triton x-100, a nonionic surfactant often used as a detergent in laboratories. This liquid mimics the dielectric characteristics of the 85-100% adipose tissue content of the normal breast tissue [34] in the considered frequency range (0.5-3 GHz), as reported in the literature [35][36]. Our measurements of the dielectric properties, shown in Fig. 2 (dashed lines), are very stable over time. Since this coupling liquid is not a mixture, it is simpler to use than the glycerin-water blend. In addition, its lower conductivity results in less attenuation for a propagating signal, which increases the signal-to-noise ratio in the measurements and may be exploited to relax the specifications of the measurement system.

We designed the antennas under the constraints of low cost, minimum size, and good matching when immersed in the selected coupling liquids. The result is a wide-band monopole antenna printed on standard FR4 dielectric substrate and provided with an SMA connector, as shown in Fig. 3(a). The printed technology minimizes fabrication costs, while the flat shape with a minimized ground plane reduces the size. In Fig. 3(b) the measured S_{11} scattering parameter (assuming a 50-Ω reference) is reported when the antenna is fully immersed in the glycerin-water coupling liquid (solid line) and in the Triton x-100 coupling liquid (dashed line). In both cases a good matching is obtained in a wide bandwidth (0.5-3 GHz).

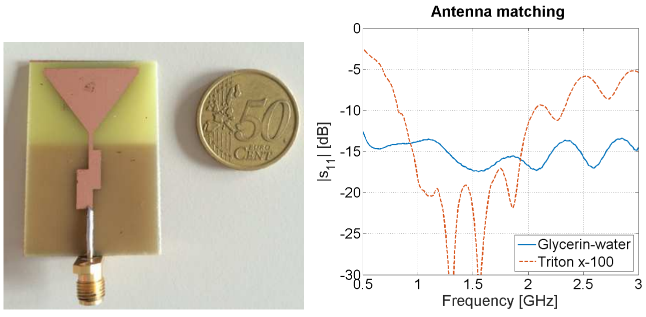

(a) **(b)**

Fig. 3. (a) Antenna and (b) S_{11} measured in 80-20% glycerin-water mixture (solid line) and in Triton x-100 (dashed line).

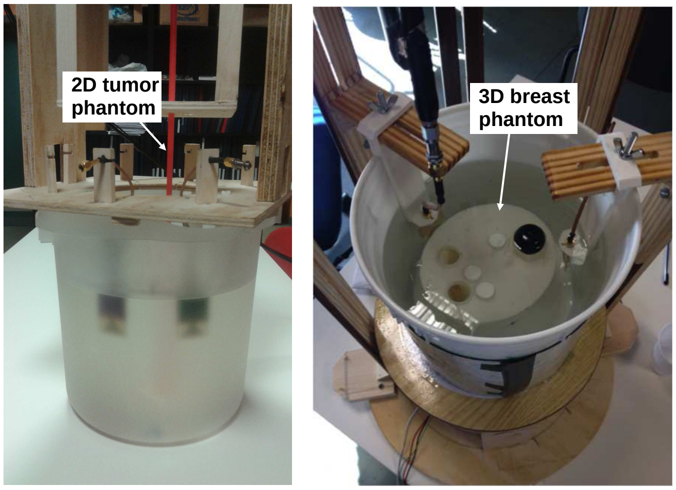

(a) **(b)**

Fig. 4. (a) First version of the tank filled with glycerin-water mixture and a vertically aligned cylinder representing a 2D tumor phantom. (b) Second version of the tank filled with Triton x-100 and a full 3D breast phantom.

We developed two versions of the tank where we mount our antennas. In the first version, shown in Fig. 4(a), the two antennas are mounted on a plexiglass support placed in the tank filled with the glycerin-water mixture. The angle between the antennas is kept fixed during the entire measurement, but it can be any multiple of 45° (the angle is 45° in Fig. 4(a)). A 2D tumor phantom is represented by either a red plastic cylinder filled with a different liquid than the coupling one (the plastic thickness is minimal and makes the cylinder transparent in the microwave range) or a metallic cylinder (not shown in figure). The cylinder can be placed in different positions. A motor placed on top of the tank rotates the cylinder along a circle in such a way to scan the entire scene. Rotating the phantom is equivalent to rotating the antennas and is much simpler in a laboratory experiment. Rotating the phantom at almost arbitrary angles gives us more flexibility than having multiple antennas in fixed positions, and can *virtualize* a very large number of antennas. Moreover, by avoiding the switch matrix needed to multiplex TX and RX among multiple antennas [14][20][31], we eliminate a further source of cost and inaccuracy. While a mechanical rotating prototype and a system based on a matrix of switches are certainly different,

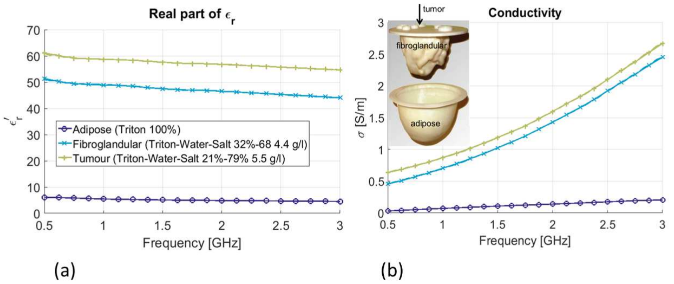

Fig. 5. GeePs-L2S phantom; (a) permittivity and (b) conductivity of the liquids used to mimic the breast tissues; inset: parts of the phantom [37].

they permit to measure the scattered field in a multitude of positions: fixed antenna positions for the matrix of switches, mobile and reconfigurable positions for the rotating system.

In the second version of the tank, shown in Fig. 4(b), we added two external wooden supports for the antennas, which permit a movement in steps along the z-axis and make it easier to change the angle between the antennas (135° in Fig. 4(b)). In this second version of the tank we experimented with a full, 3D breast-phantom that is described later in Sec. III-B. In this case the motor is placed below the tank and rotates the entire tank and so also the breast phantom in it. Like in the first version, keeping the antennas in their original position while the scene rotates is equivalent to rotating the antennas and is much simpler for a prototype.

The simple approach of rotating the phantom is appropriate for our prototype, which is not meant to be used in a clinic setting. Indeed it would be impossible to rotate the patient. In a realistic setting the patient will lay still in prone position. The tank will be placed under the patient. In this case, antennas can be attached to the tank walls and a motor can rotate together the tank and the antennas, while the patient stay still. Two additional motors can be used to move the antennas up and down for 3D measurements. Another possibility is using multiple antennas in fixed positions and a matrix of electronic switches to replace the mechanical rotation system.

B. Breast and Tumor Phantoms

In the first version of our prototype we experimented with 2D tumor phantoms represented by two different cylinders immersed in the tank filled with the 80%-20% glycerin-water mixture. The first of these two phantoms is a 12-mm diameter metallic cylinder, which mimics a highly reflective tumor. The second one is a 20-mm diameter plastic dielectric cylinder filled with a mixture of glycerin and water in different proportions than in the coupling liquid: a 40%-60% mixture, which creates with the coupling liquid a much slighter dielectric contrast (∼4:1) with respect to the metallic cylinder. The length of the cylinders is equal to the length of the whole tank. The phantom rotates while the antennas are fixed; 18 measurement positions are considered with steps of 20°. The TX and RX antennas are placed along a 20-cm diameter circle at an angle of 45° or 135° between them.

In the second version of our prototype we could experiment with the GeePs-L2S breast phantom [37], which was kindly

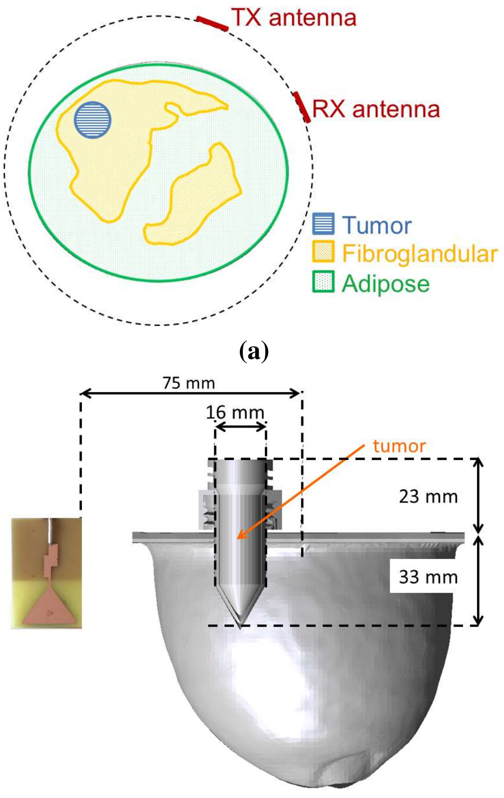

(a)

(b)

Fig. 6. GeePs-L2S breast phantom: (a) horizontal cut in the antenna plane; the outer circle represents the rotation path. (b) Cross section view showing tumor size and position. The antennas can be placed at any vertical position.

made available to us in the framework of the BMBS COST Action TD1301 “MiMed”, a project funded by the European Union and dedicated to the application of microwave imaging to medicine. The GeePs-L2S phantom represents a 3D realistic breast, fabricated with the 3D printing technology. Three different tissues, adipose, fibroglandular, and tumor, are represented by different plastic parts, as shown in the inset in Fig. 5. Each of these parts is filled with a liquid that mimics the dielectric properties of the corresponding tissue [37]. These liquids have been obtained with a proper mixture of water, salt, and Triton x-100: the measured permittivity and conductivity are reported in Fig. 5(a) and Fig. 5(b), respectively.

In the second version of the prototype, the antennas and the phantom are inside a tank filled with Triton x-100 as coupling liquid. The antennas are placed in fixed positions along a 15-cm diameter circle, at an angle of 45°, 90°, or 135° degrees between them. The phantom and the tank rotate in 24 positions with a 15-degree step.

Fig. 6(a) shows a 2D horizontal cut of the GeePs-L2S breast phantom, which corresponds to the plane where the tumor detection is performed with the I-MUSIC algorithm and where the TX and RX antennas are located (antenna plane). The dashed circle around the breast is the path along which the antennas rotate. The shape of the different tissues is represented by different patterns. Notice that the fact that the tumor is located inside the fibroglandular tissue represents an adverse condition for detection: the dielectric contrast between the two tissues is 1.2:1, much less than the contrast between fat and tumor, which is around 11:1. Fig. 6(b) depicts a cross section view of the GeePs-L2S breast phantom highlighting the size and position of the tumor. The diameter of the tumor is 16 mm. The antennas are located near the upper part of the phantom at a 75-mm distance from the phantom center as shown in Fig. 6(b).

The height at which the antennas are placed can be changed. This is an important feature of our prototype because it will allow us to perform 3D measurements as a future development.

C. RF Transceiver

In our prototype, the SoC configures the PLL-based transmitter (TX) in Fig. 1 to synthesize a frequency in the bandwidth of interest starting from a stable reference. For the TX we use a Linear Technology LTC6946 chip, an ultra-low noise and spurious PLL Integer-N synthesizer with integrated VCO (0.5-dBm output power at 1.5 GHz). A standard 10-MHz oven-controlled crystal oscillator by Golledge Electronics Ltd provides the reference frequency.

Since the LTC6946 chip does not permit to control the output power, we add the voltage-controlled VGA in Fig. 1. For this component we selected the ADL5330 by Analog Devices, which has a gain ranging from -34 to +22 dB[2].

Especially when using the glycerin-water mixture, the received signal can be very low because of the large attenuation of this coupling liquid. The addition on the receiver path of band-pass filtering (Mini-Circuits component) and low-noise amplification (LNA, gain between 15 and 10 dB in the bandwidth, 1-dB max noise figure, also by Mini-Circuits) helps increase the performance of the DC receiver. For the receiver we selected the LTM9004 chip by Linear Technology, a 14-bit DC receiver with SNR 80 dB/MHz, typical noise floor -148.3 dBm/Hz, dynamic range 86 dB, minimum detectable signal -90 dBm (-105 dBm with the LNA). The local oscillator signal (LO in Fig. 1) is provided by the transmitter itself and is attenuated (6 dB) to avoid saturation. The dynamic range of the system is coincident with that of the RF transceiver.

Linear Technology produces two boards with the TX and RX chips, respectively. Passive components mounted on these boards guarantee a good 50-Ω matching in the 1.4-1.6 GHz range both for the TX and RX. We thus selected this 200-MHz bandwidth for our experiments. The chips themselves, however, may cover a much larger bandwidth, 0.37-5.7 GHz for the TX and 0.7-2.7 GHz for the RX. Working on a wide bandwidth would require a very complicated matching network in the board and, most of all, will not result in better detection performance, as we shown later on by comparing the results obtained by our prototype with those obtained by a VNA working in the full 0.5-3 GHz bandwidth.

The digital values of the acquired signals, sampled with a 80-MHz clock, are sent via a USB-interface board to the Zynq.

---

[2] Note that even at the highest gain, according to [38] the power irradiated in the breast at the frequencies at stake and with our antennas will be within the absorption limits such as those recommended by the IEEE [39].

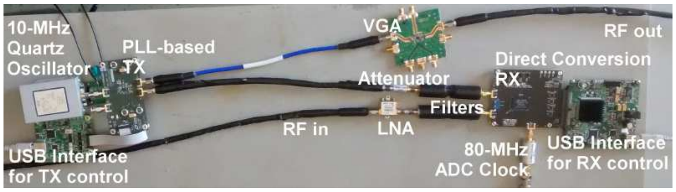

Fig. 7. Low-cost, small-size components off-the-shelf used in our system.

All components of our prototype are off-the-shelf, with the exception of the low-cost custom printed antennas. The picture in Fig. 7 encloses all the boards with the previously described RF components. Note that the cost of the COTS used in this prototype is around 3k USD. We expect a lower cost after a full engineering of an ad-hoc custom board with the same chips used in the prototype.

D. FPGA-Based Digital Back-End

The Xilinx's Zynq SoC is a decisive part toward achieving the goals of cost and form-factor reduction. Its key characteristic is the integration in the same chip of a dual-core ARM processor, which includes a level-2 cache and various standard peripherals and is denoted as *processing system (PS)* in Fig. 1, with an Artix-7 FPGA denoted as *programmable logic (PL)*.

For each frequency and antenna position, several I/Q samples are acquired by the DC receiver. As clear from Fig. 1, these 14-bit I/Q samples are sent in source-synchronous mode to the Zynq and are first buffered in a FIFO implemented in the PL part. The buffered samples are then transferred to the external DDR memory via DMA.

The processing phase starts with an average of the samples aimed at reducing noise. Then, for each frequency, the decluttering phase and eigenvalue computation are performed.The two loops where Green functions and Hermitian product are evaluated, represent the computational bottleneck. Notice that the kernel code of the loops is repeated for each pixel of the image in a 2D slice. In addition, if multiple scans along the z-axis are performed, the execution time would be multiplied by the number of such scans. For these reasons, a pure software execution of these loops may not be compatible with the duration of a medical examination. Therefore, we decided to design a hardware accelerator for these loops.

As shown in Fig. 1, the accelerator is implemented in the PL part of the Zynq. The rest of I-MUSIC runs in software in the ARM processor: the communication between the ARM and the accelerator happens via DMA. We did not describe the accelerator in RTL using a hardware description language like Verilog or VHDL. Instead, we described the accelerator in behavioral SystemC and used a commercial High-Level Synthesis (HLS) tool to obtain the RTL description, which is the entry point of the regular Xilinx FPGA design flow. With this high-level approach, we could run an extensive exploration to determine the Pareto-optimal micro-architectural solutions in the design space of performance and FPGA resources. Thanks to the HLS tool, we could validate in about four months around 100 design alternatives obtained with the application of parallelism, pipelining, loop unrolling, and other design knobs, starting from a single high-level description.

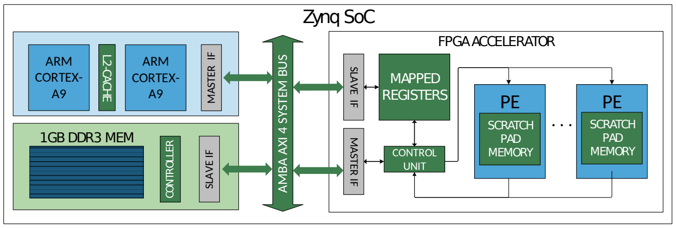

Fig. 8. I-MUSIC computing architecture on a Xilinx Zynq SoC.

Among these alternatives, we selected the accelerator outlined in Fig. 8, which consists of identical processing elements (PE) operating in parallel each on a *row* of the image. The row, as atomic processing unit, is a good balance between internal memory size of the accelerator and communication overhead. For each complex operation that a PE executes, such as division, square root, trigonometric function evaluation, etc, we obtained a high-performance, pipelined implementation using HLS. Processor-Accelerator communication does not stall the computation, because we pipelined computation and communication in such a way not to waste a single clock cycle. The accelerator has two a bus-slave interface for commands and status information, and a bus-master interface for DMA data transfers. Having performance as a goal, we synthesized the maximum number of PEs that fit on the Zynq.

The execution of the algorithm on a server-class Intel multicore (Xeon E5-2643 @3.30 GHz, 64 GB RAM) requires around 20 s, while the accelerator completes the computation in less than 1 s independently on the input data, obtaining more than 20x speed-up with respect to a software execution. If we project these results on a scenario where 3D measurements are taken (i.e. several measurements repeated at different heights), the overall measurement time is reduced from 20-30 minutes to few minutes. This is particularly important given that the patient must remain still during the measurement process.

E. System Calibration

A well-known issue of DC receivers is the offset created by the LO leakage [40]. The various contributions to the output offset, including the LO leakage, are fully compensated during the calibration phase that precedes the measurement phase. The calibration phase consists of three parts.

In the first part we do not apply the input signal nor the LO input (we replace the antenna and the LO source with two 50-Ω terminations). In this condition, the output offset is independent of the LO leakage offset. This offset is fully compensated by acting on two specific offset correction inputs of the receiver chip in the receiver board.

In the second part, we still do not apply the input signal but we consider the effect of the LO source. The offset in this case is due to the self-mixing of the LO signal that couples with the input path. Since the LO is derived from the transmitter and since its amplitude varies with frequency, we observe a different offset at each frequency. Due to this frequency dependence, this offset contribution cannot be compensated by acting on the

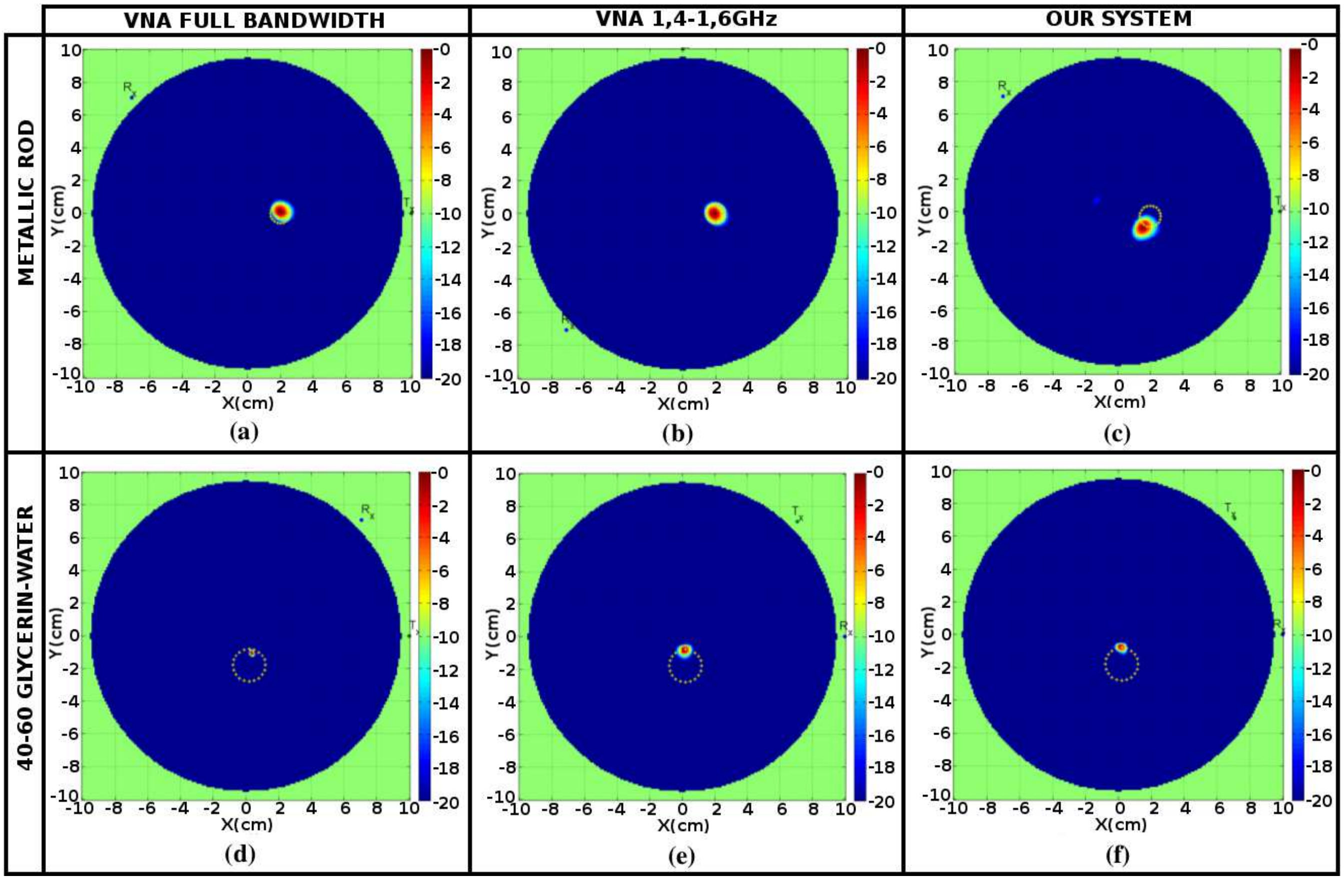

Fig. 9. Maps obtained with I-MUSIC, (a)-(c) 12-mm metallic target, (d)-(f) 20-mm cylinder filled with 40%-60% glycerin-water mixture. (a) and (d) obtained with the VNA, full bandwidth; (b) and (e) obtained with the VNA, 1.4-1.6 GHz; (c) and (f) obtained with our system.

previously mentioned offset correction inputs. It can be easily compensated, however, during the post-processing software elaboration of the acquired data, by subtracting the offset values to any measured sample, frequency by frequency.

In the third and last part of the calibration phase we apply, other than the LO source, a test input signal obtained connecting together the TX and RX cables without the antennas. The value of I/Q data acquired in this condition at different frequencies are first offset-compensated by subtracting the offset values obtained in the second part; then the so-obtained data are recorded, frequency by frequency, to be used later on as normalization values during the actual measurement. This third calibration procedure is no different than the standard calibration procedure of any VNA.

IV. EXPERIMENTAL RESULTS

The tank with the antennas and the phantoms can be connected either to our COTS-based microwave imaging system or to a broadband VNA. Therefore, we could easily compare the results obtained by running the I-MUSIC algorithm on the data acquired with our system and with the VNA.

With our system, we acquired data of the scattered field between 1.4 GHz and 1.6 GHz, which is where the receiver board is best matched, in 20-MHz steps. With the VNA, we gathered data in the same bandwidth for a fair comparison, but we could also scan the investigated scene between 0.5 and 3.0 GHz. In this way, with the first set of measurements we evaluated the accuracy of our system compared to the VNA, and with the second one we assessed if relevant information is lost when considering only the 1.4-1.6 GHz range.

A. *First Tank Version*

Fig. 9 shows the images obtained after running I-MUSIC on the data acquired with the first version of the measurement tank. The figure is a visual representation of the reconstructed image with the tumor position. The yellow circle identifies the position and size of the tumor phantom, while the colored shades highlight the scattering points detected by the algorithm. When the scattered points detected and the yellow circle overlap, or are at least in close proximity, it means that the algorithm successfully detected the tumor.

Figs. 9(a)-(c) refer to the case of the metallic cylinder. In this case the angle between the antennas was 135°. Figs. 9(a)-(b) are obtained with the VNA in the full range and in the sub-range between 1.4 and 1.6 GHz, respectively: we do not observe a significant loss of information. Fig. 9(c) shows that our system correctly detects the target, only slightly shifted.

Figs. 9(d)-(f) are obtained with the dielectric cylinder. The angle between the antennas was 45°. In this case, additional frequencies in the full range slightly improve the focus of the detected point, as we can see by comparing Fig. 9(d), obtained with the VNA in the full range, with Fig. 9(e), obtained in the

The final version of record is available at http://dx.doi.org/10.1109/TBCAS.2017.2703588

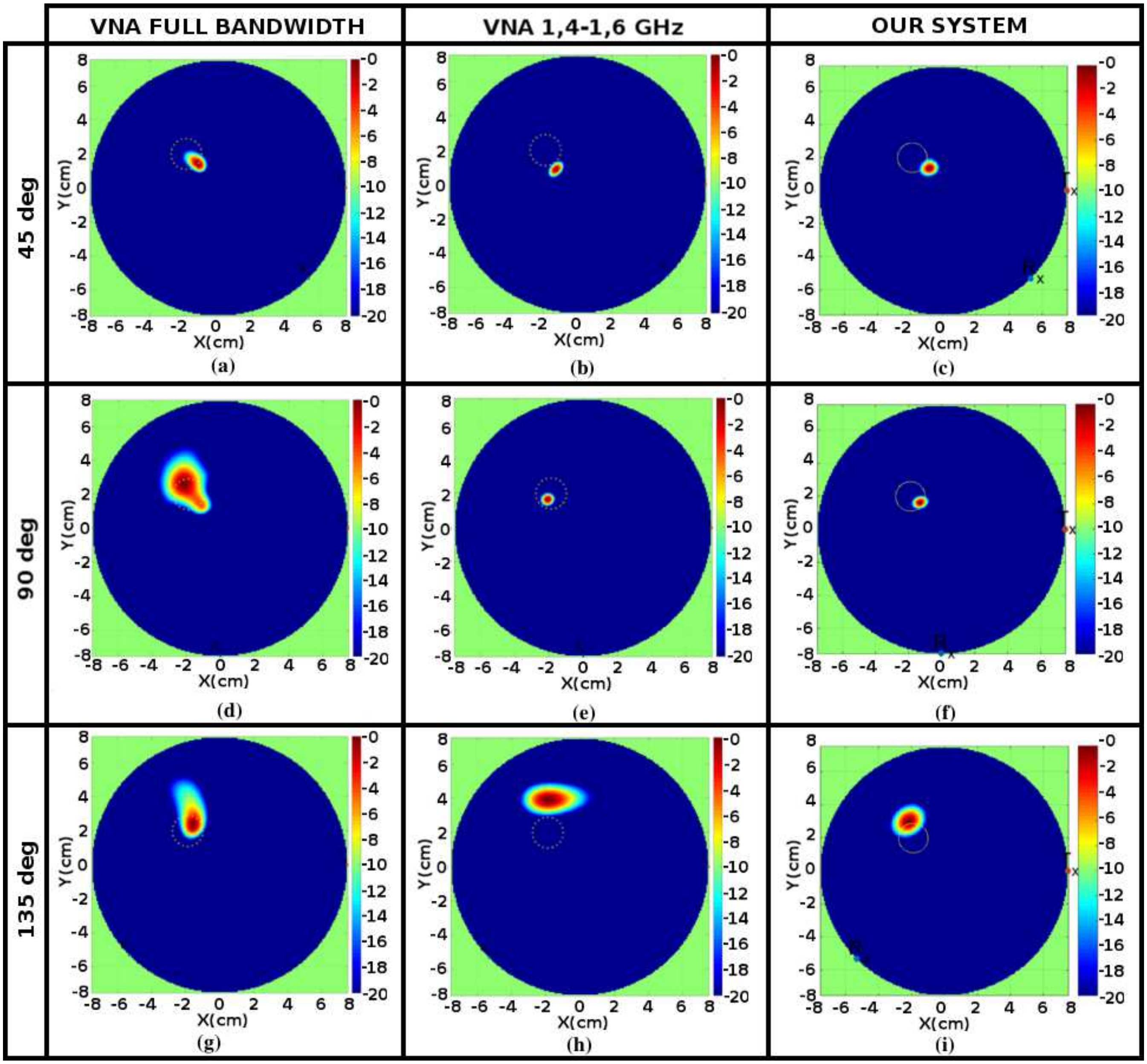

Fig. 10. Maps obtained with I-MUSIC using the GeePs-L2S breast phantom; the angle between the TX and RX antennas is 45° in the first row (a-c), 90° in the second row (d-f), and 135° in third row (g-i); in the first column (a,d,g) the VNA is used in the 0.5-3 GHz range; in the second column (b,e,h) the VNA is used in the 1.4-1.6 GHz range; in the third row (c,f,i) our system is used in the 1.4-1.6 GHz range.

1.4-1.6 GHz range. Fig. 9(f) shows that our system correctly detects the target, with a focus similar and marginally better than what the VNA obtains in the same frequency range.

B. Second Tank Version

Fig. 10 reports the results obtained on the data gathered with the second version of our prototype and the GeePs-L2S breast phantom. Each row corresponds to a different angle between the TX and RX antennas (45°, 90°, and 135°). The yellow circle represents the actual position and size of the tumor.

The first two columns are obtained with the VNA in the full bandwidth and in the 1.4-1.6 GHz range, respectively. The third column is obtained instead with our COTS-based system.

We notice that in this more realistic scenario, the reconstructions are characterized by some delocalization, which in turn depends on the angle between the TX and RX antennas. This is caused by the inevitable model mismatch between the equivalent permittivity of the I-MUSIC algorithm and the actual profile in the detection scene.

Nonetheless, the tumor is clearly detected. This is a remarkable result in view of the low contrast between the tumor and the surrounding fibroglandular tissue and because the tumor is embedded within the fibroglandular structure. Also, the experiments show that working in the full bandwidth leads to worse results (first vs. second column): the tumor, albeit detected, is not as focused as in the 1.4-1.6 GHz range. (In Secs. IV-C and IV-D we discuss the effect of the fibroglandular tissue and the bandwidth more in depth.) By comparing the results obtained in this range with the VNA and with our system (second vs. third column), we conclude that the results are similar, and a slightly better focus is actually obtained by our system in the 135-degree case.

To further compare the results obtained by the VNA and our system, we report in Tab. I the values of Signal-to-Mean Ratio (SMR) and Signal-to-Clutter Ratio (SCR) [16] obtained in each case of Fig. 10. The values of SMR and SCR are generally higher for our system than for the VNA, with the exception of the case when the angle between the antennas is 90° which is unexpectedly good for the VNA.

TABLE I
SMR AND SCR OBTAINED WITH THE GEEPS-L2S BREAST PHANTOM IN A TRITON COUPLING MEDIUM, VARYING THE ANTENNA ANGLE.

	VNA full bandwidth		VNA 1.4-1.6 GHz		Our system 1.4-1.6 GHz	
Angle (deg)	**SMR (dB)**	**SCR (dB)**	**SMR (dB)**	**SCR (dB)**	**SMR (dB)**	**SCR (dB)**
45	47.8	30.4	52.0	29.4	53.8	32.7
90	30.7	28.4	56.3	92.9	55.6	68.0
135	36.8	41.1	34.9	38.9	42.4	57.1

C. Effect of Fibroglandular Tissue

By comparing Fig. 9 with Fig. 10, a loss of resolution can be noticed in Fig. 10, especially for the measurements with the VNA at full bandwidth and at an angle of 135°. We conjecture that this is mainly an effect of the fibroglandular tissue, for which we offer in the following a possible explanation.

Since I-MUSIC is a subspace projection method, the scatterer's location is identified where the modeled Green function forms a zero angle with the dominant eigenvector of the correlation matrix $\mathbf{R}$. An error in the model makes it impossible to meet the zero angle condition, which results in a loss of resolution, as it happens in Fig. 10. Such error depends on many parameters, including: how the actual permittivity of the breast differs from the model, the aspect angle between the transmitting and receiving antennas (which involves different paths of propagation inside the breast and therefore a different model error), and the adopted frequency band. As for the latter point, we remark that increasing the frequency band not necessarily improves the quality of the reconstruction. This is due to the lossy characteristics of the involved tissues, which get worse with frequency: since the model is lossless, its error increases with frequency; moreover, the scattered field is attenuated and so more corruptible by uncertainties. This explains the unexpected behavior of the method as the frequency band increases (less resolution in the first column of Fig. 10). If losses were accounted for and assuming that noise does not overwhelm data, performance would improve. More details can be found in [41].

To provide an experimental evidence, we removed the fibroglandular structure from the phantom. Figs. 11(a)-11(b) report the reconstruction obtained with bands 0.3-5 GHz and 1.4-1.6 GHz, respectively, and at a 90-degree angle. Fig. 11(c) reports the scattering measurements across the different sensors positions (lines at different colors) as a function of the frequency. The resolution improves when the full bandwidth is used compared to the results in Fig. 10, because now the error of the model is lower. However, Fig. 11(b) is still better resolved. Fig. 11(c) clarifies that this happens because weaker high-frequency data are more corrupted by uncertainties.

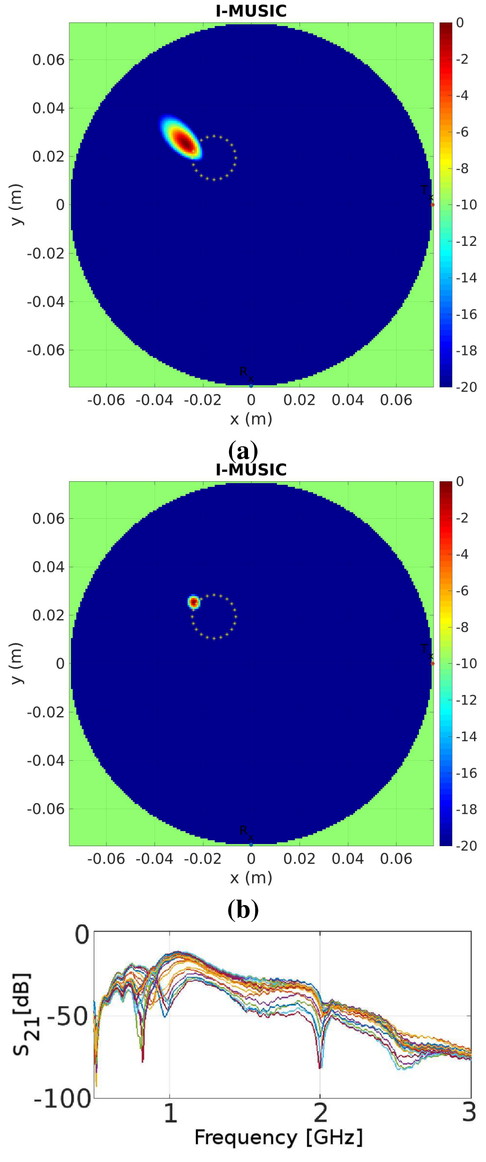

(a)
(b)
(c)

Fig. 11. GeePs-L2S breast phantom without the fibroglandular structure: Maps obtained with I-MUSIC in (a) full bandwidth and (b) 1.4-1.6 GHz; (c) scattering measurements across the different sensors positions (lines with different colors) as a function of the frequency.

D. Discussion on Resolution

In standard microwave imaging algorithms (e.g. beamforming, time-reversal, and the like) the achievable resolution, i.e. the ability to resolve two distinct points in the image, improves as the bandwidth increases. In non-standard imaging methods, however, the role of bandwidth is weak. When full-view measurements are available (i.e. sensors can run all around the scattering scene) it is even possible to improve the resolution with an increasingly smaller bandwidth. In these

The final version of record is available at http://dx.doi.org/10.1109/TBCAS.2017.2703588

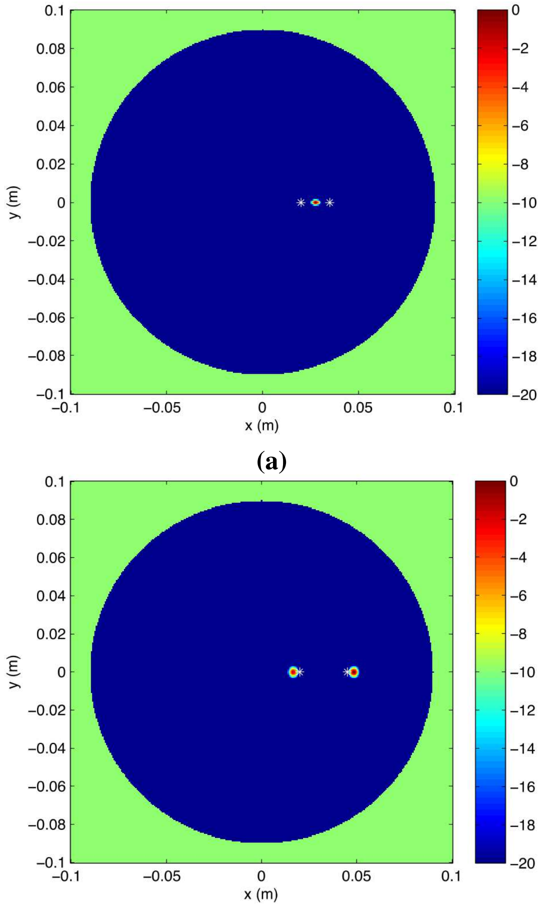

(a)

(b)

Fig. 12. Maps obtained with I-MUSIC over a simulation of two scatterers located at a distance (a) equal to and (b) two times greater than the minimum distance corresponding to the algorithm (distance) resolution. The two sources are detected incorrectly in (a) and correctly in (b).

cases, frequency allocation plays a key role, not only the bandwidth [42]. Note that I-MUSIC is a variant of Time-Reversal MUSIC, which is known to obtain a much finer resolution than standard methods do even if it works at a single frequency (i.e. bandwidth is null) [43]. Using data obtained at multiple frequencies, however, can be beneficial. This is particularly true for I-MUSIC, in which multiple frequencies help mitigate the rank deficiency of the correlation matrix $\mathbf{R}$, especially when more than one scatterer is in the scene [41]. In summary, with I-MUSIC there are no theoretical obstacles to obtaining a high resolution even with the relatively small 200-MHz bandwidth that we used in our work.

Indeed, the presence of more than one strong scatterer in the scene can be a source of resolution degradation. We do not have measurements for such a case since the phantom in the current form does not allow us to test this condition. Therefore, we report in Fig. 12 simulation results obtained at the highest frequency of our system (1.6 GHz) and using for simplicity a homogeneous lossless background with relative dielectric permittivity equal to 10. The theoretical analysis proposed in [41] suggests that the achievable resolution is 2.4/k=2.2 cm where k is the background wave number. To check this, we simulated two scatterers located at a 2.2-cm distance and at a distance two times this value. The simulation results confirm the theoretical prediction: both scatterers are detected in the latter case, as shown in Fig. 12(b), whereas Fig. 12(a) shows that in the former case only one scatterer is found in the midpoint of the segment linking the two scatterers.

For what concerns the minimum detectable tumor size, we remark that I-MUSIC inherits the properties of Time-reversal MUSIC, which in ideal conditions is known to detect point-like scatterers (i.e. dimensionless) working at a single frequency, provided that the number of spatial measurement exceeds the number of point-like scatterers. Therefore, unlike standard methods, I-MUSIC can theoretically detect very small scatterers without using a large bandwidth. Under non-ideal conditions, however, the minimum detectable tumor size depends on model and measurements uncertainties, noise, and hardware limitations. A *sufficiently large* field scattered by the tumor is needed under these conditions. Even though we leave the quantification of how large the scattered field needs to be to future developments, we remark that in the previous works on I-MUSIC a 5-mm tumor was considered [25][26]. We also remark that the size of the tumor phantom used in this work is in line with the average size of a Ductal Carcinoma in-situ (DCIS) lesion, which is the most commonly detected early-stage breast cancer, 10-15 mm, according to the Surveillance, Epidemiology and End Results Data (SEER) [44].

Finally, we comment on the unambiguous range. For a standard radar system this would be related to the pulse repetition frequency (in time domain) or to the frequency step (using the SFCW approach). Since we do not use a standard imaging method, what matters is the highest adopted frequency and the number of spatial measurements (i.e. the antennas in our case). Assume for simplicity a homogeneous breast. This hypothesis simplifies the discussion but at the same time represents a non-favorable situation for ambiguities as a mismatch between the model used in the construction of the steering vector and the real scenario is actually helpful for mitigating uniqueness problems [45]. By adapting the derivation presented in [41] to the scattering scenario at hand, it can be shown that to avoid ambiguities in the reconstruction the number of antennas must be greater than $4 \times k_{\max} \times R_b$, R_b being the breast radius and $k_{\max}$ the wave number (in the coupling medium) at the highest adopted frequency. At the highest frequency that we use, this constraint is easily satisfied because we use 16 antenna measurements, which is more than the minimum ($\sim$13 measurements).

V. CONCLUSIONS

We presented a low-cost, fast, and accurate system for breast cancer detection using microwave imaging. The system is low-cost because it uses components off-the-shelf and in-house fabricated antennas. It is fast because it executes the imaging algorithm more than 20x faster than a multicore CPU thanks to the use of FPGA hardware acceleration. Finally, our experimental results show that detection is possible with accuracy similar to what can be achieved using standard costly microwave equipment such as a vector network analyzer.

The theory behind I-MUSIC tells us that in ideal conditions point-like scatterers can be detected; hence one next step in this research activity is to verify the minimum size of a detectable scatterer in non-ideal conditions, preparing a proper phantom that allows us to perform this investigation. We are also planning to replace the mechanical rotating system with a matrix of electronic switches as a further step toward clinical experiments.

ACKNOWLEDGMENT

We wish to thank Prof. N. Joachimowicz and Prof. B. Duchêne of Paris-Sud University for making available the GeePs-L2S breast phantom under the MiMed collaborative framework. We thank Prof. P. Palmero of Politecnico di Torino for her help with the preparation of the liquids required to mimic different tissues.

REFERENCES

[1] E. C. Fear, P. M. Meaney, and M. A. Stuchly, "Microwaves for breast cancer detection?" *IEEE Potentials*, vol. 22, no. 1, pp. 12–18, Feb 2003.

[2] R. Figueras, J. Sabadell, L. Teres, and F. Serra-Graells, "A 70-mu m pitch 8-mu w self-biased charge-integration active pixel for digital mammography," *IEEE Transactions on Biomedical Circuits and Systems*, vol. 5, no. 5, pp. 481–489, Oct 2011.

[3] D. Liang, H. T. Hui, T. S. Yeo, and B. K. Li, "Stacked phased array coils for increasing the signal-to-noise ratio in magnetic resonance imaging," *IEEE Transactions on Biomedical Circuits and Systems*, vol. 7, no. 1, pp. 24–30, Feb 2013.

[4] B. Sarioglu, M. Tumer, U. Cindemir, B. Camli, G. Dundar, C. Ozturk, and A. D. Yalcinkaya, "An optically powered cmos tracking system for 3 t magnetic resonance environment," *IEEE Transactions on Biomedical Circuits and Systems*, vol. 9, no. 1, pp. 12–20, Feb 2015.

[5] S. M. Sohn, L. DelaBarre, A. Gopinath, and J. T. Vaughan, "Design of an electrically automated rf transceiver head coil in mri," *IEEE Transactions on Biomedical Circuits and Systems*, vol. 9, no. 5, pp. 725–732, Oct 2015.

[6] P. M. Meaney, M. W. Fanning, D. Li, S. P. Poplack, and K. D. Paulsen, "A clinical prototype for active microwave imaging of the breast," *IEEE Trans. Microw. Theory Techn.*, vol. 48, no. 11, pp. 1841–1853, 2000.

[7] A. Martellosio, M. Pasian, M. Bozzi, L. Perregrini, A. Mazzanti, F. Svelto, P. E. Summers, G. Renne, and M. Bellomi, "0.5-50 GHz dielectric characterisation of breast cancer tissues," *Electronics Lett.*, vol. 51, no. 13, pp. 974–975, 2015.

[8] P. Meaney, "Microwave imaging and emerging applications," *Int. Journal of Biomed. Imag.*, vol. v.2012, May 2012.

[9] S.Kwon and S.Lee, "Recent advances in microwave imaging for breast cancer detection," *Int. Journal of Biomed. Imag.*, vol. v.2016, December 2016.

[10] Y. Xing, K. D. Cromwell, and J. N. Cormier, "Review of diagnostic imaging modalities for the surveillance of melanoma patients," *Dermatology Research and Practice*, vol. 2012, no. 4, pp. 12–6, 2012.

[11] S. Brovoll, T. Berger, Y. Paichard, . Aardal, T. S. Lande, and S. E. Hamran, "Time-lapse imaging of human heart motion with switched array uwb radar," *IEEE Transactions on Biomedical Circuits and Systems*, vol. 8, no. 5, pp. 704–715, Oct 2014.

[12] S. C. Hagness, A. Taflove, and J. E. Bridges, "Two-dimensional FDTD analysis of a pulsed microwave confocal system for breast cancer detection: Fixed-focus and antenna-array sensors," *IEEE Trans. Bio-Med. Eng.*, vol. 45, no. 12, pp. 1470–1479, 1998.

[13] A. Arbabian, S. Callender, S. Kang, B. Afshar, J. C. Chien, and A. M. Niknejad, "A 90 GHz hybrid switching pulsed-transmitter for medical imaging," *IEEE J. Solid-State Circuits*, vol. 45, no. 12, pp. 2667–2681, Dec 2010.

[14] A. Azhari, S. Takumi, S. Kenta, T. Kikkawa, and X. Xiao, "A 17 GHz bandwidth 1.2 mW CMOS switching matrix for UWB breast cancer imaging," in *Proc. IEEE BioCAS*, 2014, pp. 109–112.

[15] Y. Seo, K. Sogo, A. Toya, T. Sugitani, A. Azhari, X. Xiao, and T. Kikkawa, "CMOS equivalent time sampling of gaussian monocycle pulse for confocal imaging," in *Proc. IEEE BioCAS*, 2014, pp. 125–128.

[16] X. Guo, M. R. Casu, M. Graziano, and M. Zamboni, "Simulation and design of an UWB imaging system for breast cancer detection," *Integration, the VLSI Journal*, vol. 47, no. 4, pp. 548–559, 2014.

[17] E. J. Bond, X. Li, S. C. Hagness, and B. D. Van Veen, "Microwave imaging via space-time beamforming for early detection of breast cancer," *IEEE Trans. Antennas Propag.*, vol. 51, no. 8, pp. 1690–1705, 2003.

[18] M. Bassi, A. Bevilacqua, A. Gerosa, and A. Neviani, "Integrated SFCW transceivers for UWB breast cancer imaging: Architectures and circuit constraints," *IEEE Trans. Circuits Syst. I*, vol. 59, no. 6, pp. 1228–1241, 2012.

[19] M. Bassi, M. Caruso, M. S. Khan, A. Bevilacqua, A. D. Capobianco, and A. Neviani, "An integrated microwave imaging radar with planar antennas for breast cancer detection," *IEEE Trans. Microw. Theory Techn.*, vol. 61, no. 5, pp. 2108–2118, May 2013.

[20] M. Klemm, J. Leendertz, D. Gibbins, I. J. Craddock, A. Preece, and R. Benjamin, "Microwave radar-based differential breast cancer imaging: imaging in homogeneous breast phantoms and low contrast scenarios," *IEEE Trans. Antennas Propag.*, vol. 58, no. 7, pp. 2337–2344, 2010.

[21] H. Wi, H. Sohal, A. L. McEwan, E. J. Woo, and T. I. Oh, "Multi-frequency electrical impedance tomography system with automatic self-calibration for long-term monitoring," *IEEE Transactions on Biomedical Circuits and Systems*, vol. 8, no. 1, pp. 119–128, Feb 2014.

[22] A. McEwan, J. Tapson, A. van Schaik, and D. S. Holder, "Code-division-multiplexed electrical impedance tomography spectroscopy," *IEEE Transactions on Biomedical Circuits and Systems*, vol. 3, no. 5, pp. 332–338, Oct 2009.

[23] S.-H. Son, N. Simonov, H.-J. Kim, J.-M. Lee, , and S.-I. Jeon, "Pre-clinical prototype development of a microwave tomography system for breast cancer detection," *ETRI Journal*, vol. 32, no. 6, pp. 901–910, Dec 2010.

[24] T. M. Grzegorczyk, P. M. Meaney, P. A. Kaufman, R. M. di Florio-Alexander, and K. D. Paulsen, "Fast 3-D tomographic microwave imaging for breast cancer detection," *IEEE Trans. Med. Imag.*, vol. 31, no. 8, pp. 1584–1592, 2012.

[25] G. Ruvio, R. Solimene, A. Cuccaro, and M. J. Ammann, "Comparison of noncoherent linear breast cancer detection algorithms applied to a 2-D numerical model," *IEEE Antennas Wireless Propag. Lett.*, vol. 12, pp. 853–856, 2013.

[26] G. Ruvio, R. Solimene, A. Cuccaro, D. Gaetano, J. E. Browne, and M. J. Ammann, "Breast cancer detection using interferometric music: Experimental and numerical assessment," *Medical Physics*, vol. 41, no. 103101, pp. 1–11, 2014.

[27] D. J. Pagliari, A. Pulimeno, M. Vacca, J. A. Tobon Vasquez, F. Vipiana, M. R. Casu, R. Solimene, and L. P. Carloni, "A low-cost, fast, and accurate microwave imaging system for breast cancer detection," in *Proc. IEEE BioCAS*, 2015.

[28] J. A. Tobon Vasquez, F. Vipiana, G. Dassano, M. R. Casu, M. Vacca, A. Pulimeno, and R. Solimene, "Experimental results on the use of the MUSIC algorithm for early breast cancer detection," in *Int. Conf. on Electromagnetics in Advanced Applications (ICEAA)*, 2015.

[29] J. A. Tobon Vasquez, E. Attardo, G. Dassano, F. Vipiana, M. R. Casu, M. Vacca, A. Pulimeno, and G. Vecchi, "Design and modeling of a microwave imaging system for breast cancer detection," in *9th European Conf. Antennas Propag. (EuCAP)*, 2015.

[30] X. Zeng, A. Fhager, Z. He, M. Persson, P. Linner, and H. Zirath, "Development of a time domain microwave system for medical diagnostics," *IEEE Trans. Instrum. Meas.*, vol. 63, no. 12, pp. 2931–2939, Dec 2014.

[31] A. Azhari, T. Sugitani, X. Xiao, and T. Kikkawa, "DC-17-GHz CMOS single-pole-eight-throw switching matrix for radar-based image detection," *Japanese Journal of Applied Physics*, vol. 55, no. 12, p. 127301, Dec. 2016.

[32] Q. Li, X. Xiao, L. Wang, H. Song, H. Kono, P. Liu, H. Lu, and T. Kikkawa, "Direct extraction of tumor response based on ensemble empirical mode decomposition for image reconstruction of early breast cancer detection by UWB," *IEEE Trans. Biomed. Circuits Syst.*, vol. 9, no. 5, pp. 710–724, Oct 2015.

[33] P. M. Meaney, F. Shubitidze, M. W. Fanning, M. Kmiec, N. R. Epstein, and K. D. Paulsen, "Surface wave multipath signals in near-field microwave imaging," *Int. Journal of Biomed. Imag.*, vol. 2012, 2012.

[34] M. Lazebnik, L. McCartney, D. Popovic, C. B. Watkins, M. J. Lindstrom, J. Harter, S. Sewall, A. Magliocco, J. H. Booske, M. Okoniewski, and S. C. Hagness, "A large-scale study of the ultrawideband microwave dielectric properties of normal breast tissue obtained from reduction surgeries," *Phys Med Biol.*, vol. 52, no. 10, pp. 2637–2656, Apr 2007.

[35] S. Romeo, L. Di Donato, O. M. Bucci, I. Catapano, L. Crocco, M. R. Scarfi, and R. Massa, "Dielectric characterization study of liquid-based materials for mimicking breast tissues," *Microwave and Optical Technology Letters*, vol. 53, no. 6, pp. 1276–1280, June 2011.

[36] N. Joachimowicz, C. Conessa, T. Henriksson, and B. Duchene, “Breast phantoms for microwave imaging,” *IEEE Antennas Wireless Propag. Lett.*, vol. 13, pp. 1333–1336, 2014.
[37] N. Joachimowicz, B. Duchene, C. Conessa, O. Meyer, and O. Dubrunfaut, “Easy-to-produce stable-in-time 3d-printed breast phantoms for microwave imaging,” in *PIERS*, 2015.
[38] N. Johnson and T. Takenaka, “Preliminary assessment of electromagnetic absorption in the breast for cylindrical microwave breast cancer detection systems,” in *PIERS*, 2006, pp. 256–260.
[39] *IEEE Recommended Practice for Radio Frequency Safety Programs, 3 kHz to 300 GHz*, IEEE Std. C95.7-2014, August 2014.
[40] B. Razavi, *RF Microelectronics*. Upper Saddle River, NJ: Prentice-Hall, 1998.
[41] R. Solimene, G. Ruvio, A. Dell’Aversano, A. Cuccaro, M. Ammann, and R. Pierri, “Detecting point-like sources of unknown frequency spectra,” *Progress In Electromagnetics Research*, vol. B, no. 50, pp. 347–364, 2013.
[42] R. Solimene, A. Cuccaro, G. Ruvio, D. F. Tapia, and M. O’Halloran, “Beamforming and holography image formation methods: an analytic study,” *Opt. Express*, vol. 24, no. 8, pp. 9077–9093, Apr 2016.
[43] S. Lehman and A. Devaney, “Trasmission mode time-reversal super-resolution imaging,” *The Journal of the Acoustical Society of America*, vol. 113, no. 5, pp. 2742–2753, June 2003.
[44] M. Mossa-Basha, G. Fundaro, B. AShah, S. Ali, and M. Pantelic, “Ductal carcinoma in situ of the breast: MR imaging findings with histopathologic correlation,” *RadioGraphics*, vol. 30, no. 6, pp. 1673–1687, October 2010.
[45] A. J. Devaney, “Time reversal imaging of obscured targets from multi-static data,” *IEEE Trans. Antennas Propag.*, vol. 53, no. 5, pp. 1600–1610, May 2005.

Mario R. Casu received the laurea degree *summa cum laude* in electronics engineering and the Ph.D. degree in electronics and communications engineering from the Politecnico di Torino, Torino, Italy, in 1998 and 2001, respectively. He is currently an associate professor in the Department of Electronics and Telecommunications of the Politecnico di Torino. Among his current research interests are Systems-on-Chip with specialized accelerators, Networks-on-Chip, and circuits, systems, and platforms for biomedical applications. He regularly serves as a reviewer for peer-reviewed journals and in the technical program committee of international conferences.

Marco Vacca received the Ph.D. degree in Electronics and Communications engineering from the Politecnico di Torino, Turin, Italy, in 2013. He is now an Assistant Professor at the Politecnico di Torino. His research activities include modeling and design of integrated circuits (digital, mixed-signal and RF) and prototyping on field-programmable gate arrays (FPGA). He is also an expert of innovative and unconventional computer architectures and beyond-CMOS technologies. He is currently involved in two national projects on microwave imaging technology, one for early breast cancer detection and the other one for brain stroke monitoring.

Jorge A. Tobon received the degree in electronics engineering at the Universidad de Antioquia, Colombia in 2010, he also completed the Master Degree in Electronic Engineering at the Politecnico di Torino in the same year. He received the Ph.D. degree in electronics and telecommunication engineering from the Politecnico di Torino, Italy, in 2014. In 2014 he worked as a researcher at the Istituto Superiore Mario Boella, and since 2015 he is working at the Politecnico di Torino as a post-doc researcher. His main research interests are the development of numerical techniques for integral equations, the study and modeling of electromagnetic propagation in non-homogeneous media, the analysis of radio communications between space re-entry vehicles and ground stations, and modelling, design and analysis of systems for microwave imaging applications.

Azzurra Pulimeno Azzurra Pulimeno received the Master degree in Electronics Engineering and the PhD in Electronics and Communications Engineering both from the Politecnico di Torino, Italy. Her research activities involve the analysis and modeling of new quantum technologies for digital computation (e.g. molecular QCA and molecular FET), the design and simulation of nanoelectronics circuits, the prototyping and testing of a system for breast cancer detection.

Imran Sarwar recieved his Bachelors degree in Electrical Engineering from Baluchistan University of Engineering and Technology Khuzdar, Pakistan, in 2012. He then received his Master in Electronic Engineering from the Politecnico di Torino, Italy in 2015 and then he started his PhD in November 2015 at Politecnico di Torino. He is working on Microwave imaging and hardware accelerators in FPGAs. Imran Sarwar was the only scholar who won scholarship offered by higher Education (HEC) of Pakistan from his region for his bachelor studies and then he was also awarded scholarship from HEC for 5 years for MS leading to PhD.

Raffaele Solimene received the laurea degree (summa cum laude) in 1999 and the Ph.D. degree in 2003 in electronic engineering, both from the Seconda Universit di Napoli (SUN), Aversa, Italy. In 2002, he became assistant professor at the Faculty of Engineering of the University Mediterranea of Reggio Calabria, Italy. Since 2006, he has been with the Dipartimento di Ingegneria Industriale e dellInformazione at the University of Campania “Luigi Vanvitelli”) (former SUN) where he is currently associate professor. He serves as associate editor for International Journal of Antennas and Propagation and for Mathematical Problems in Engineering. His research activities focus on inverse problems with applications to nondestructive subsurface investigations, through-the-wall imaging and breast cancer detection.

Francesca Vipiana received the Master Degree and the Ph.D. in Electronic Engineering from Politecnico di Torino, Turin, Italy, in 2000 and 2004, respectively, with doctoral research carried out partly at the European Space Research Technology Centre (ESTEC), Noordwijk, The Netherlands. Since 2012, she has been with the Department of Electronics and Telecommunications, Politecnico di Torino, as an Assistant Professor, and from 2014 as an Associate Professor. Her research interests include numerical techniques based on the integral equation (IE), method of moments (MoM) approaches, with focus on multiresolution (MR) and hierarchical schemes, domain decomposition, preconditioning and fast solution methods, Greens function regularization, and advanced quadrature integration schemes. She is also involved in the analysis, synthesis and optimization of multi-band reconfigurable compact antennas, and in the modeling and design of microwave imaging systems for medical applications.